Performance of the Global Forecast System's Medium-Range Precipitation Forecasts in the Niger River Basin Using Multiple Satellite-Based Products

Haowen Yue[1], Mekonnen Gebremichael[1], and Vahid Nourani[2,3]

[1] Department of Civil and Environmental Engineering, University of California, Los Angeles, CA 90095-1593
[2] Faculty of Civil Engineering, University of Tabriz, Tabriz, Iran
[3] Near East University, Faculty of Civil and Environmental Engineering, Near East Boulevard, 99138, Nicosia, via Mersin 10, Turkey

Correspondence to: Mekonnen Gebremichael (mekonnen@seas.ucla.edu)

Abstract. Accurate weather forecast information has the potential to improve water resources management, energy, and agriculture. This study evaluates the accuracy of medium-range (1 – 15 day) precipitation forecasts from the Global Forecast System (GFS) over watersheds of eight major dams (Selingue Dam, Markala Dam, Goronyo Dam, Bakolori Dam, Kainji Dam, Jebba Dam, Dadin Kowa Dam, and Lagdo Dam) in the Niger river basin using NASA's Integrated Multi-satellitE Retrievals (IMERG) "Final Run" satellite-gauge merged rainfall observations. The results indicate that the accuracy of GFS forecast varies depending on climatic regime, lead time, accumulation timescale, and spatial scale. The GFS forecast has large overestimation bias in the Guinea region of the basin (wet climatic regime), moderate overestimation bias in the Savannah region (moderately wet climatic regime), but has no bias in the Sahel region (dry climate). Averaging the forecasts at coarser spatial scales leads to increased forecast accuracy. For daily rainfall forecasts, the performance of GFS is very low for almost all watersheds except for Markala and Kainji dams, both of which have much larger watershed areas compared to the other watersheds. Averaging the forecasts at longer time scales also leads to increased forecast accuracy. The GFS forecasts, at 15-day accumulation timescale, have better performance, but tend to overestimate high rain rates. Additionally, the performance assessment of two other satellite products was conducted using IMERG Final estimates as reference. The Climate Hazards Group InfraRed Precipitation with Station data (CHIRPS) satellite-gauge merged product has similar rainfall characteristics with IMERG Final, indicating the robustness of IMERG Final. The IMERG "Early Run" satellite-only rainfall product is biased in the dry Sahel region, however in the wet Guinea and Savannah regions, IMERG "Early Run" outperforms GFS in terms of bias.

1. Introduction

Global climate forecasts, with lead times ranging from hours to several months, are becoming increasingly available (Saha et al. 2014; Abdalla et al. 2013; NCEP 2015; JMA 2019). Significant societal benefit could be realized from research to reduce common barriers in climate forecast utilization blocking the path to improving water resources management, energy, and agriculture. One such a barrier is the lack of understanding of climate forecast accuracy in different regions of the world. This focus is timely given the recent advances in numerical atmospheric models, and in the wealth of new observing capabilities including satellite remote sensing. These combined models and observational datasets provide opportunity for researchers to quantify the accuracy of climate forecasts.

The Niger River is the principal river of West Africa, and is shared among nine riparian countries (Fig. 1): Benin, Burkina Faso, Cameroon, Chad, Guinea, Ivory Coast, Mali, Niger and Nigeria. The basin is facing multiple pressures from increasing population, water abstraction for irrigation, and risk of extreme hydrological events due to climate change (Sylla et al. 2018). A number of hydropower dams exist in the region, and additional dam projects are envisaged in order to alleviate chronic power shortages in the countries of the Niger basin. Optimal management of water resources is key to maximizing benefits, such as hydropower generation, and minimize disasters, such as flooding. Climate forecast information has the potential to improve water resources management, energy, and agriculture (e.g., Patt et al. 2007; Breuer et al. 2010; Mase and Prokopy 2014; Pandya et al. 2015; Koppa et al. 2019; Alexander et al. 2020). For example, in a recent study, Koppa et al (2019) showed that the use of seasonal precipitation forecasts in reservoir planning of Omo Gibe dam in Ethiopia can increase annual hydropower generation by around 40%.

Several studies have investigated the accuracy of seasonal forecasts in West Africa (e.g., Bliefernicht et al. 2019; Pirret et al. 2020). Seasonal forecasts are important for water resource planning, while medium-range (1-day to 15-day) forecasts are important for operational decisions, such as reservoir operations. The availability of medium-range global climate forecasts has grown in recent years. Examples of such forecast products include Global Forecast System (GFS; NCEP 2015), NCEP climate forecast system (NSF CFS, Saha et al. 2014), European Centre for Medium-Range Weather Forecasts (ECMWF; Abdalla et al. 2013), and Global Spectral Model (GSM; JMA 2019). For these precipitation forecasts to be effectively used in applications, their accuracy must be known, which is usually performed
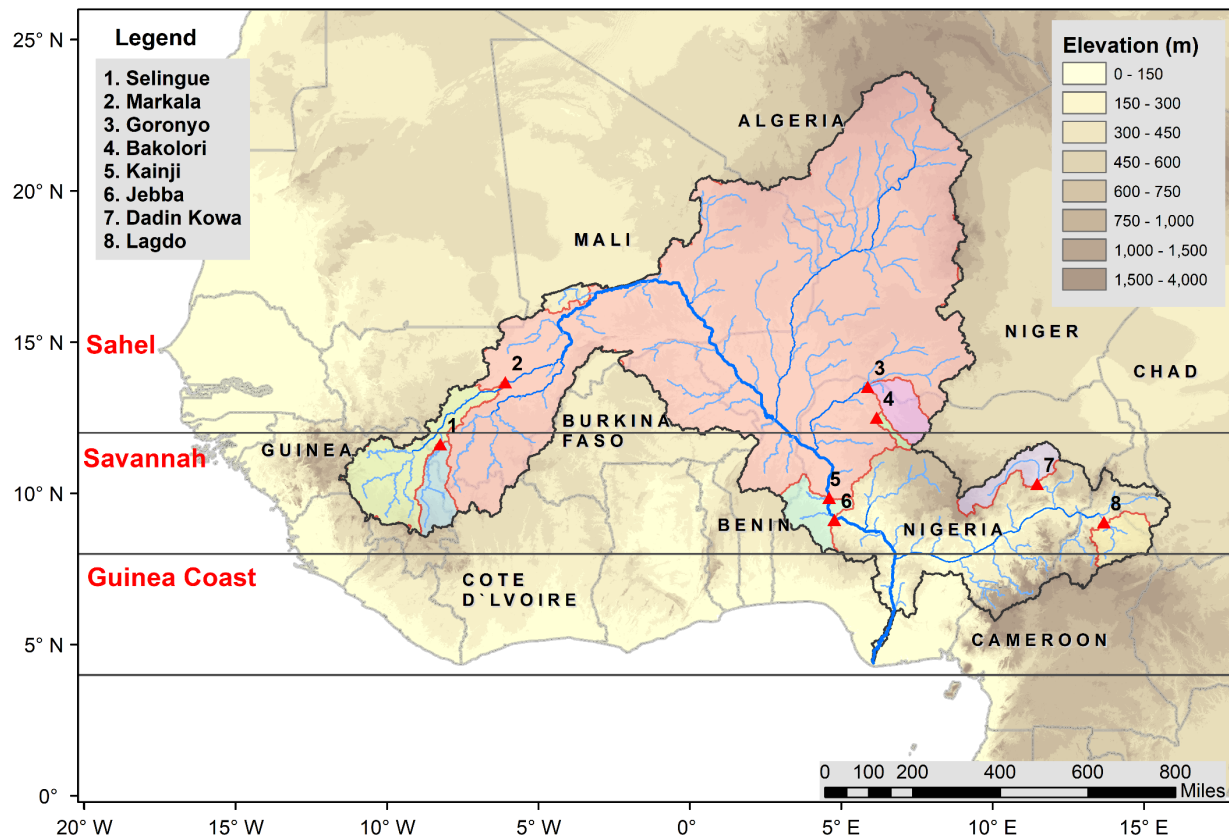
3

Figure 1. The Niger River Basin, and locations of major reservoir dams in the basin: (1) Selingue, (2) Markala, (3) Goronyo, (4) Bakolori, (5) Kainji, (6) Jebba, (7) Dadin Kowa, and (8) Lagdo.

62   through comparison of precipitation forecasts to observations (e.g., Tian et al. 2017; Yuan et al. 2014). Wang et al.

63   (2019) performed numerical experiment to examine the sensitivity of GFS to inclusion or exclusion of additional

64   observations collected over the eastern Pacific during the El Niño Rapid Response (ENRR) field campaign, type of

65   data assimilation method to prepare the initial conditions, and inclusion or exclusion of stochastic parameterizations

66   in the forecast model. They reported that the GFS forecast errors are only slightly sensitive to the additional ENRR

67   observations, more sensitive to the DA methods, and most sensitive to the inclusion of stochastic parameterizations in

68   the model. In addition, they reported that GFS forecasts have difficulty to capture the location and magnitude of heavy

69   rain rates. Sridevi et al. (2018) evaluated the performance of GFS in India by using rain gauge and satellite rainfall

70   product, and reported that the GFS forecast shows some skills in 1-day and 2-day lead times, but low skills from 3-

71   day onwards. Lien et al. (2016) compared the statistical properties of GFS forecasts and Tropical Rainfall Measuring

72   Mission (TRMM) Multisatellite Precipitation Analysis (TMPA; Huffman et al. 2007, 2010) observations. They

73   reported that the GFS model has positive bias in precipitation amount compared to TMPA observations, and that the

4

74 GFS forecasts have large random errors at higher resolutions, especially for convective precipitation. According to

75 Jiang et al. (2015) the lack of consideration of the Aerosol-Cloud Interactions (ACIs) in the GFS model leads to

76 significant bias in the GFS precipitation forecasts.

77

78 In our study region of the Niger River basin, there has not been any performance evaluation of GFS precipitation

79 forecasts to date. The Niger basin lies in three different climate regimes (wet regime, moderately wet regime, and dry

80 regime), and is home to nine major irrigation and hydropower dams (Selingue, Markala, Goronyo, Bakolori, Kainji,

81 Jebba, Dadin Kowa, and Lagdo). Recent advances in satellite rainfall products, particularly following the Global

82 Satellite Measurement satellite mission (GPM; Hou et al. 2014), and extensive evaluation of GPM rainfall products

83 in West Africa, provides us with opportunity to use GPM rainfall products as reference for evaluation. Many studies

84 have conducted to evaluate the accuracy of the satellite rainfall estimates in West Africa. Dezfuli et al. (2017a)

85 evaluated the performance of NASA's Integrated Multi-satellitE Retrievals (IMERG) "Final Run" (IMERG Final)

86 (version 4; Huffman et al. 2019a, b) in comparison with two, high-resolution, experimental rain gauge station data

87 provided by the Trans-African Hydro-Meteorological Observatory (TAHMO; van de Giesen et al. 2014), and reported

88 the capability of IMERG Final to represent well the diurnal cycle of rainfall. Using the same dataset, Dezfuli et al.

89 (2017b) showed that IMERG Final is able to capture the propagation of large Mesoscale Convective Systems (MCSs),

90 a significant advantage over its predecessor's (TMPA) 3-hourly temporal resolution, which misses the time evolution

91 of most of these systems. Gossett et al. (2018) evaluated the performance of a number of satellite rainfall products

92 (focusing only on versions that do not include rain gauge data) by comparison with rain gauge station networks in

93 Benin and Niger, and reported that the satellite products (especially IMERG Early) exhibit high performance in Niger

94 but relatively lower performance in Benin. Satgé et al. (2020) evaluated the accuracy of a number of gridded

95 precipitation datasets over West Africa through comparison against rain gauge station data, and reported that CHIRPS

96 and TMPA (the predecessor to IMERG) provided reliable estimates at both daily and monthly timescales, while the

97 remaining satellite products considered (CMORPH, PERSIANN, GSMaP, ARC, and TAMSAT) and all atmospheric

98 reanalysis products considered (MERRA and JRA) were deemed unreliable. Furthermore, they found out that satellite

99 products that incorporated rain gauge information outperformed satellite-only products. Maranan et al. (2020)

100 compared IMERG Final products against experimental rain gauge station data in the moist forest region of Ghana,

101   West Africa, and showed that IMERG Final datasets are able to capture monthly rainfall with a correlation coefficient

102   close to unity.

103

104   The objective of this study is to evaluate the accuracy of medium-range precipitation forecasts derived from the Global

105   Forecast System (GFS) for the major reservoir dams of the Niger basin through comparison against IMERG Final.

106   We chose GFS model due to its relatively high spatial (0.25° x 0.25°) and temporal resolution (3-hourly to 6-hourly)

107   as well as free-of-charge data availability to users. The main questions addressed in this study are as follows. First,

108   how does the accuracy of GFS forecast vary across different reservoir dams in the same basin? Second, how does the

109   accuracy vary with lead time in the range 1- to 15-day? Third, what is the effect of spatial averaging (from 0.25° all

110   the way to basin-scale) and temporal aggregation (from 1-day to 15-day) on the forecast accuracy? Fourth, how does

111   the accuracy of GFS forecast compare with the accuracy of satellite-only rainfall products that are available in near-

112   real-time, as the latter may have the potential to calibrate and improve the accuracy of GFS?

113

114   **2.   Data and Methodology**

115   **2.1 Global Forecast System (GFS) Medium-Range Precipitation Forecasts**

116

117   The Global Forecast System (GFS) is a global numerical weather prediction system run by the U.S. National Weather

118   Service (NWS). The GFS forecast products with a resolution of 0.25° by 0.25° are obtained from National Center for

119   Atmospheric Research (NCAR) Research Data Archive (RDA) GFS Historical Archive (NCEP 2015). The GFS is

120   run four times a day at UTC 00, UTC 06, UTC 12, and UTC 18 hours. One of the GFS model output variables is

121   accumulated precipitation, where the precipitation forecasts are accumulations starting from the model run time. We

122   obtained the 1-day lead daily rainfall forecast by subtracting the 24-hour rainfall accumulation forecast from the 48-

123   hour rainfall accumulation forecast. Similarly, in order to obtain the 5-day lead daily rainfall forecast, we subtracted

124   the 120-hour rainfall accumulation forecast from the 144-hour rainfall forecast. We only considered the model runs at

125   UTC 00 hour.

126

127   The GFS model went through a major upgrade, and its version-15 forecasts are available since June 12, 2019. In

128   version 15, the Finite Volume Cubed Sphere dynamical model (FV3) replaced the Global Spectral Model (GSM) as

the core model. In the GSM model, the horizontal resolutions were T1543 (12.5km) from 0 to 240 hours (0-10 days) and T574 (~34km) from 240 to 384 hours (10-16 days) (NCEP 2021a). However, in the FV3 model, the horizontal resolution of the model is about 13 km for days 0-16 (NCEP 2021b). The model runs are re-gridded to produce precipitation forecasts at 0.25° resolution (NCEP 2015). The Key FV3 model schemes include (Putman and Lin 2007): (1) the Rapid Radiative Transfer Method for GCMs (RRTMG) scheme for shortwave/longwave radiation (Mlawer et al. 1997; Iacono et al. 2000; Clough et al. 2005), (2) the Hybrid eddy-diffusivity mass-flux (EDMF) scheme for Planetary Boundary Layer (PBL) (NCEP, 2021a), (3) the Noah Land Surface Model (LSM) scheme for land surface option (Chen et al. 1997), (4) the Simplified Arakawa-Schubert (SAS) deep convection for cumulus parameterization (Arakawa et al. 1974; Grell 1993), and (5) an advanced GFDL microphysics scheme for microphysics (NCEP, 2021b).

2.2 IMERG Final Satellite Precipitation Products

IMERG Final rainfall products are used in this study as reference to evaluate the performance of GFS precipitation forecasts. IMERG Final combines all available microwave precipitation estimates, microwave-calibrated infrared estimates, and rain gauge data to provide rainfall estimates at very high resolution (30-minute, 0.10°) (Hou et al. 2014; Huffman et al. 2015). The IMERG products are categorized into three types, namely early run, late run, and final run. It is only the final run or "final" version that incorporates rain gauge data. The data latency of IMERG Final is about 3.5 months. Details of IMERG algorithm developed by NASA are available at Huffman et al (2019a, b). The latest version (V6B) of IMERG datasets have been accessed from the NASA's Earth Data Goddard Earth Sciences Data and Information Services Center (GES DISC) web portal.

2.3 Other Satellite Precipitation Products

In order to put the GFS forecast performance into perspective, we also evaluated two other state-of-the-art satellite rainfall products:

- IMERG Early provides un-calibrated IMERG rainfall fields, which do not include correction from rain gauges. The data latency of IMERG Early is near-real-time, about 4 hours. We have used the latest version (V6B) of IMERG Early datasets. Post-processing calibration of GFS forecasts (in order to improve the accuracy of GFS forecasts) requires the use of "relatively better performing" and "available in near-real-time" independent rainfall observations to correct real-time dynamical GFS model forecasts. Comparison of the performance of

157   IMERG Early with the performance of GFS would indicate to what extent the IMER Early products could be

158   used for calibration of GFS forecasts.

159   •   The Climate Hazards Group InfraRed Precipitation with Station data (CHIRPS) is derived primarily from

160   thermal infrared data using the cold cloud duration (CCD) approach, calibrated using TRMM Multi-satellite

161   Precipitation analysis (TMPA 3B42 v7; Huffman et al. 2007) precipitation datasets by local regression, and

162   include rain gauge station data from multiple sources (regional and national meteorological services). CHIRPS

163   data are available at a spatial resolution of 0.05° and a temporal resolution of 1-day, with a data latency period

164   of about 3 weeks. Details of CHIRPS algorithm are available at Funk et al. (2015). Agreement between the

165   reference (IMERG Final) and CHIRPS would indicate that the IMERG Final estimates are robust.

166

167   **2.4 Study Region**

168   The Niger river, with a drainage basin of 2,117,700 Km^2, is the third longest river in Africa. The source of the main

169   river is in the Guinea Highlands, and runs through Mali, Niger, on the border with Benin and then through Nigeria,

170   discharging through a massive delta, known as the Niger Delta (the world's third largest wetland), into the Atlantic

171   Ocean. The rainfall regimes in the region follow the seasonal migration of the Inter-Tropical Convergence Zone

172   (ITCZ), which brings rainfall primarily in the summer season (Animashaun et al. 2020; Sorí et al. 2017).

173   Climatologically, the Niger basin lies in three latitudinal sub-regions (Akinsanola et al. 2015, 2017): (1) the Guinea

174   coast (latitude 4°–8°N), which borders the tropical Atlantic Ocean in the south; (2) the Savannah (latitude 8°–12°N),

175   an intermediate sub-region; and (3) the Sahel (latitude > 12°N) to the north. The Guinea coast experiences a

176   bimodal rainfall regime that is centered in the summer monsoon period of June–September, with August being the

177   period of a short dry season, while the Savannah and Sahel sub-regions experience a unimodal rainfall regime, with

178   maximum rainfall occurring in August (Akinsanola and Zhou 2018). The ranges of annual rainfall amounts are: 400–

179   600 mm in the Sahel, 900–1200 mm in the Savannah; and 1500–2000 mm in the Guinea coast (Akinsanola et al.

180   2017).

181

182   The Niger basin is home to eight major reservoir dams (see Table 1 and Fig. 1): (1) Selingue Dam in Mali: a primarily

183   hydropower dam, (2) Markala Dam in Mali: a primarily irrigation dam, serving about 75,000 ha of farmland, (3)

184   Goronyo Dam in Nigeria: a multi-purpose dam for flood control, provision of downstream water supply and the release

185 of water for irrigation in the dry season, (4) Bakolori Dam in Nigeria: a primarily irrigation dam with a command area

186 of about 23,000 ha, (5) Kainji Dam in Nigeria: the largest Dam on the Niger supplying power for most towns in

187 Nigeria, (6) Jebba Dam in Nigeria: a primarily hydropower dam, (7) Dadin Kowa Dam: a multi-purpose dam for

188 water supply, electricity and irrigation, (8) Lagdo Dam in Cameroon: a multi-purpose dam providing electricity to the

189 northern part of the country and supplying irrigation water for 15,000 hectares of cropland. The watersheds of the

190 dams are primarily either in the Savanna (Selingue, Markala, Jebba, Dadin Kowa, an Lagdo), or in the Sahel (Goronyo,

191 Kainji), or partly in both (Bakolori). The watershed sizes vary over a large range, from 4,887 Km^2 (Bakolori Dam) to

192 1,464,092 Km^2 (Kainji Dam). The average elevations of the watersheds are close to each other at 500 ± 50 m.a.s.l.

193

194 In order to make the results of this study meaningful to reservoir managers, the Niger basin was divided into

195 watersheds according to the locations of the dam reservoirs (see Fig. 1). Then the sub-basin of each dam was defined

196 as the drainage between the dam itself and the upstream dam. For example, the drainage basin of the Markala Dam

197 does not include the drainage basin of the Selingue Dam.

198

199 Table 1. Selected dams and their watershed characteristics

| Dam | Country | Operational since* | Capacity (million m³)* | Power (MW)* | Primary Purpose* | | | Area of Drainage Basin (km²)** | Elevation of Drainage Basin (m)** |
					Irrigation and Water Supply	Flood Control	Hydroelectricity		
Selingue	Mali	1982	2170	44			x	32685	473
Markala	Mali	1947	175		x			102882	442
Goronyo	Nigeria	1983	942		x	x		31547	446
Bakolori	Nigeria	1978	450		x			4887	519
Kainji	Nigeria	1968	15000	960			x	1464092	406
Jebba	Nigeria	1984	3600	540			x	40268	308
Dadin Kowa	Nigeria	1988	2855	35	x		x	32936	535
Lagdo	Cameroon	1983	7800	72		x	x	31352	452

200 * information obtained from the Global Reservoir and Dam Database (Lehner et al. 2011) and Food and Agriculture Organization
201 of the United Nations (FAO)'s Global Information System on Water and Agriculture (AQUASTAT).
202 ** Calculated from HydroSEHDS (Lehner et al. 2008).
203
204
205 **2.5 Evaluation**

206 IMERG Final rainfall products are used in this study as reference to evaluate the performance of GFS precipitation

207 forecasts. The comparison period is 15 June 2019 to 15 June 2020 to match the period for which the version-15 of

208   GFS model forecasts is available. The spatial resolutions of the forecast and satellite products are different: 0.25°(GFS),

209   0.10° (IMERG Final and IMERG Early), and 0.05° (CHIRPS). The temporal resolutions of the satellite products are:

210   30-minute (IMERG Final and IMERG Early) and daily (CHIRPS). Our comparison is mostly based on sub-basin (i.e.

211   watershed for each dam) average values, in which case we average all the datasets to the sub-basin spatial scale. In

212   some cases, where we compare the spatial patterns of rainfall, we resample both IMERG products and CHIRPS to

213   0.25° using the bilinear interpolation technique to match the spatial resolution of GFS.

214

215   For evaluation metrics, we used the modified Kling-Gupta Efficiency (KGE; Gupta et al. 2009; Kling et al. 2012) and

216   its components: Bias Ratio (BR), correlation (R), and variability ratio (γ). *KGE* measures the goodness-of-fit between

217   estimates of precipitation forecasts and reference observations as:

218    $$KGE = 1 - \sqrt{(R-1)^2 + (BR-1)^2 + (\gamma-1)^2},$$

219    $$BR = \frac{\mu_f}{\mu_o},$$

220 $$\gamma = \frac{CV_f}{CV_o},$$

221   where R is the linear correlation coefficient between forecasted and observed precipitation, BR is the bias ratio, γ is

222   the variability ratio, μ is the mean precipitation, CV is the coefficient of variation, and the indices *f* and *o* represent

223   forecasted and observed precipitation values, respectively. KGE values range from -∞ to 1, with values closer to 1

224   indicating better model performance. Towner et al. (2019) suggested the following classifications: "Good" (KGE ≥

225   0.75), "Intermediate" (0.75 ≥ KGE ≥ 0.5), "Poor" (0.5 ≥ KGE > 0), and "Very poor" (KGE ≤ 0). The *BR* values

226   greater than 1 indicate a positive bias whereby forecasts overestimate precipitation relative to the observed data,

227   while values less than 1 represent an underestimation. *The γ values greater than 1 indicate that the variability in the

228   forecast time series is higher than that observed, and values less than 1 show the opposite effect. The *R* measures the

229   strength and direction of the linear relationship between the forecast and observed values, and to what extent the

230   temporal dynamics of observed rainfall is captured in the forecasts. The correlation values of 0.6 or more are

231   considered to be skillful (e.g., Alfieri et al. 2013). In addition, the root mean-square-error normalized by reference

232   precipitation mean (NRMSE) was also used.

233

234   **3.   Results and Discussion**

235   **3.1 Annual Spatial Variability and Seasonal Characteristics**

236   The spatial map of annual (15 June 2019 – 15 June 2020) rainfall from the various rainfall products is given in Figure

237   2. According to the reference rainfall product (i.e. IMERG Final), the Niger basin experiences average annual rainfall

238   of 700 mm. The spatial rainfall distribution shows north-to-south increasing gradient, with the Sahel region (> 12°N)

239   receiving on average 346 mm per year, the Savanna region (8°N – 12°N) receiving on average 1,206 mm per year,

240   and the Guinea region (4°N – 8°N) receiving on average 1,620 mm per year. The spatial structures (climatology and

241   north-south gradient in rainfall) of GFS, IMERG and CHIRPS rainfall fields are quite similar to those of IMERG

242   Final. However, the 1-day GFS tends to overestimate in the wet Guinea region of the basin, whereas both IMERG

243   Early and CHIRPS give values that are very close to IMERG Final.
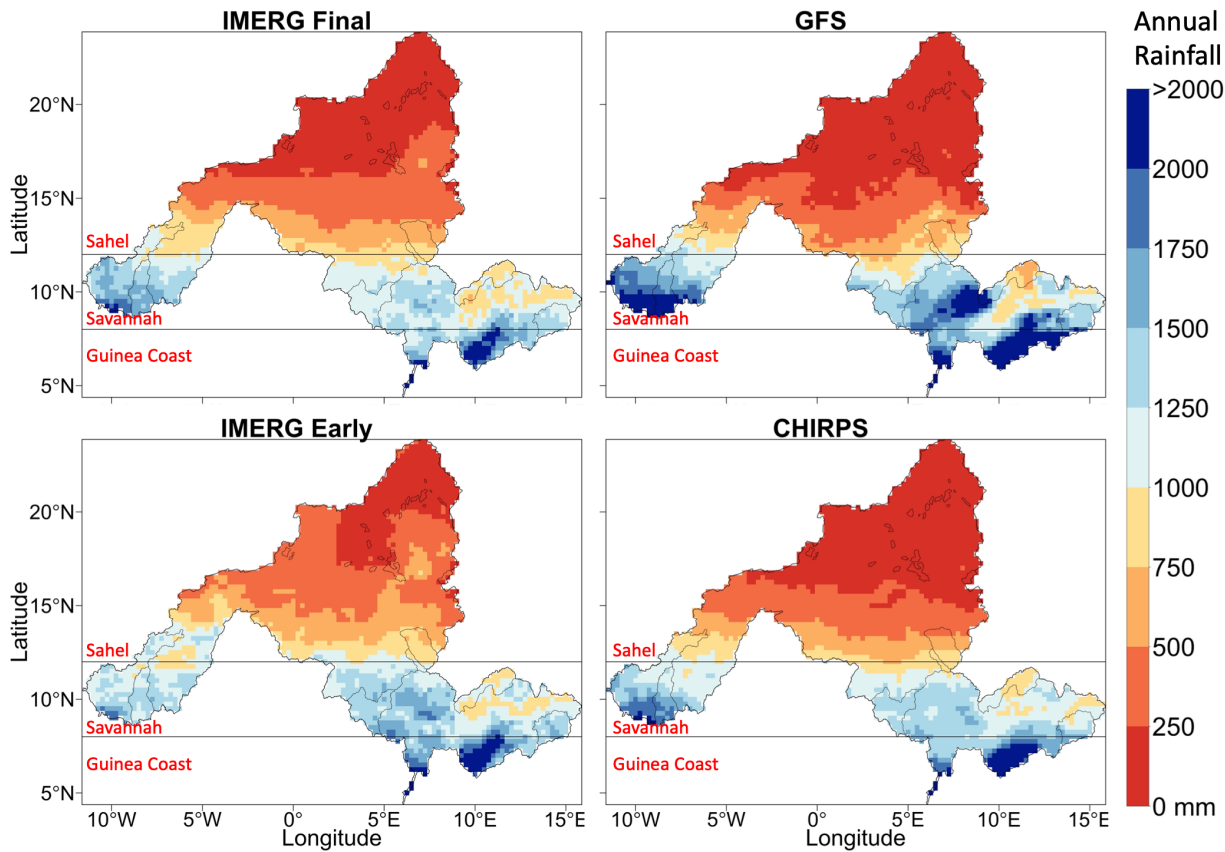
244
245   Figure 2. Spatial map of annual rainfall (in mm), for the period 15 June 2019 to 15 June 2020, derived from (a)
246   IMERG Final, (b) GFS (1-day lead time), (c) IMERG Early, and (d) CHIRPS.
247

11

248   Figure 3 shows the seasonal rainfall pattern for each climatological region. According to the reference IMERG Final,

249   as one goes from north to south, the rainy season expands from 3 months (June – September) in the Sahel to 6 months

250   (March – November) in the Savanna and Guinea regions. The peak rainfall also shows north-south gradient, with peak

251   rainfall of 130 mm in the Sahel, to 269 mm in the Savanna, and 350 mm in the Guinea. The rainfall pattern is unimodal

252   with a peak rainfall value in August for both Sahel and Savanna, but becomes bimodal with one peak in May and the

253   other in September for Guinea.

254
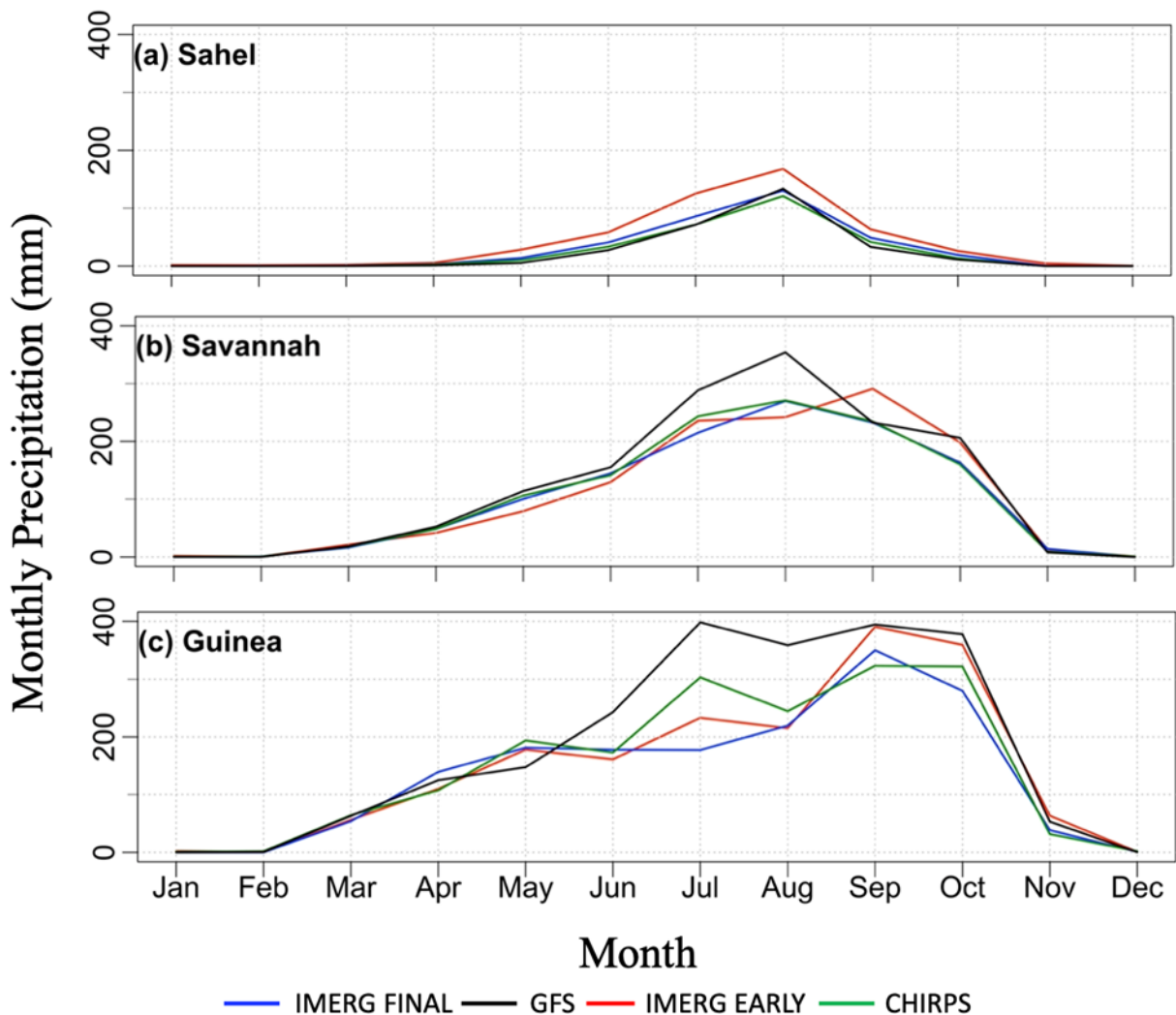
255   Figure 3. Monthly precipitation regime for the three climatological zones of the Niger river Basin: (a) Sahel, (b) Savanna, and (c) Guinea. Analyses are based on rainfall fields derived from IMERG Final, 1-day-lead GFS. IMERG Early, and CHIRPS. The time period covers from 15 June 2019 to 15 June 2020.

256

257

258   When validated against IMERG Final, the performance of GFS in capturing the seasonal rainfall characteristics

259   deteriorates as one goes from north to south. GFS captures both the seasonal rainfall pattern and rainfall peak in the

260   Sahel, and captures the seasonal rainfall pattern but tends to moderately overestimate the peak in the Savannah, while

261   it has large overestimation (almost twice as much as the reference) in the Guinea particularly during summer. As far

262   as the other satellite products are concerned, IMERG Early tends to slightly overestimate in the Sahel across all rainy

263   months, but performs relatively well in the Savannah and Guinea regions. CHIRPS is very close to IMERG Final in

264   all regions and months, with the exception of modest overestimation of the July rainfall in Guinea.

265

266   **3.2 How well do GFS forecasts capture annual rainfall?**

267   Here, we aggregate the 1-day lead GFS forecasts to annual time scale and compare the results against corresponding

268   annual precipitation estimates from IMERG Final. Figure 4 presents the watershed-averaged annual rainfall for each

269   dam watershed. According to IMERG Final, the annual rainfall varies from 434 mm (in Kainji) to 1,481 mm (in

270   Selingue). Watersheds 1 (Selingue) and 2 (Markala), located in the western part of the Savannah, receive the largest

271   amount of rainfall, i.e., 1481 mm and 1406 mm, respectively. Watershed 3 (Markala), located in the eastern part of

272   the Sahel, receives 741 mm of annual rainfall. Watershed 4 (Bakolori), characterized by the smallest watershed area

273   compared to the rest of the watersheds, lies partly in the Sahel and partly in the Savannah region and receives 921 mm

274   of annual rainfall. Watershed 5 (Kainji), characterized by the largest watershed area of all, lies mostly in the Sahel

275   region and receives the lowest amount of annual rainfall (434 mm). Watersheds 6 (Jebba), 7 (Dadin Kowa), and 8

276   (Lagdo), located in the Savannah, receive annual rainfall amounts of 1190 mm, 941 mm, and 1295 mm, respectively.

277

278   Validated against IMERG Final, the GFS tends to overestimate rainfall in all watersheds located in the Savannah (or

279   watersheds that receive relatively large rainfall amounts), with an overestimation varying in the range 8% to 33%,

280   with larger bias for watersheds receiving higher rainfall amount. For watersheds in the Sahel (watersheds receiving

281   low rainfall amount), GFS gives less bias (-11% for the driest Kainji watershed and +10% for Bakolori).

282

283   In contrast, IMERG Early tends to underestimate rainfall in all watersheds located in the Savannah (with larger

284   negative bias in watersheds with large rainfall amount) but tends to overestimate in all watersheds located in the Sahel

285   (with very large overestimation bias for the driest watershed) Therefore, GFS and IMERG Early have different bias

characteristics: whereas GFS outperforms IMERG Early in the Sahelian climate where well-organized convective systems dominate the monsoon, IMERG Early outperforms GFS in the Savannah and Guinea climate which are characterized by short-lasting and localized systems and wet land surface conditions. CHIRPS estimates are reasonably close to IMERG Final, indicating that the choice of reference product between CHIRPS and IMERG Final would not substantially affect the findings on the accuracy of GFS forecasts.
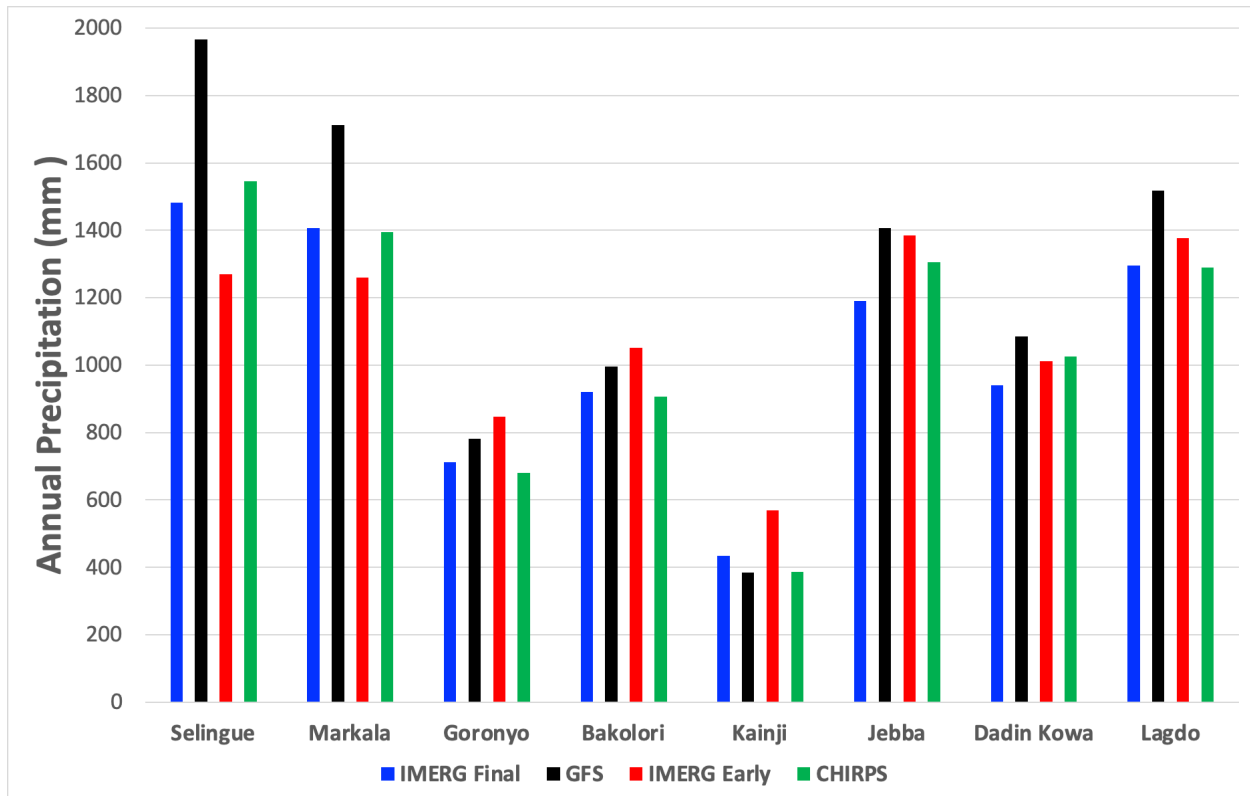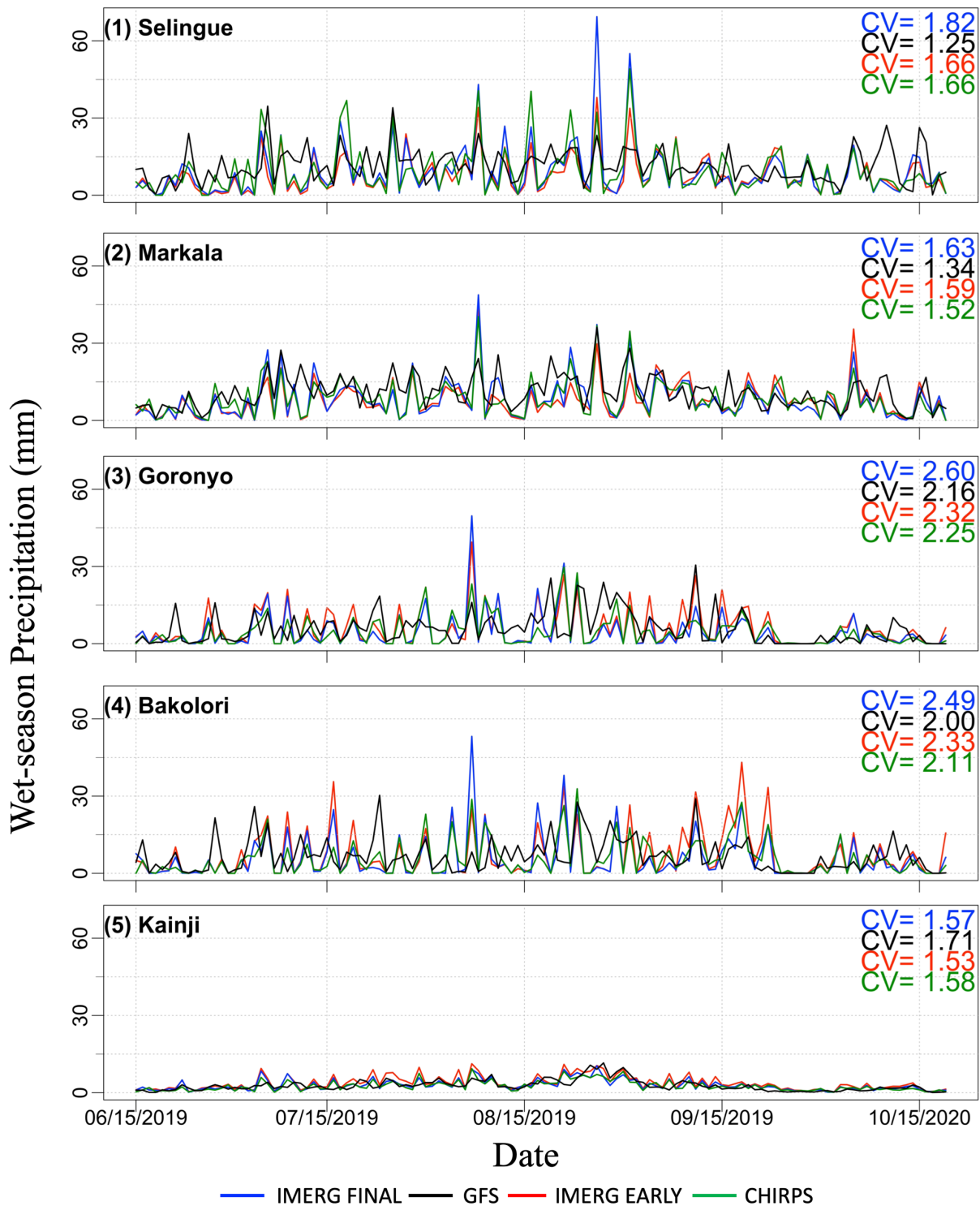

Figure 4. Sub-basin averaged annual precipitation (mm) for the period, 15 June 2019 to 15 June 2020, for each of the Niger's sub-basin, derived from the 1-day lead GFS forecast and different satellite precipitation products.

3.3 How well is the time series of daily precipitation forecasted?

Figures 5 and 6 present the time series of watershed-averaged daily rainfall, for the wet period June – October. According to IMERG Final, the temporal variability (as measured through coefficient of variation or CV) varies from 1.22 to 2.60. Validated against IMERG Final, the GFS tends to underestimate the temporal variability and particularly underestimate large spikes in rainfall, at almost all sites except at Kainji. The GFS's relatively better performance for

301   Kainji could be attributed to the watershed's large area that results in relatively smooth temporal variability. Both

302   IMERG Early and CHIRPS provide CV values that are very close to IMERG Final.

303   Figure 5. Time series of sub-basin averaged precipitation total (mm) for the wet period (June – September 2019 for
304   all sub-basins, derived from various precipitation products, for five sub-basins. The Figure also shows the
305   coefficient of variation (CV) as a measure of temporal variation.
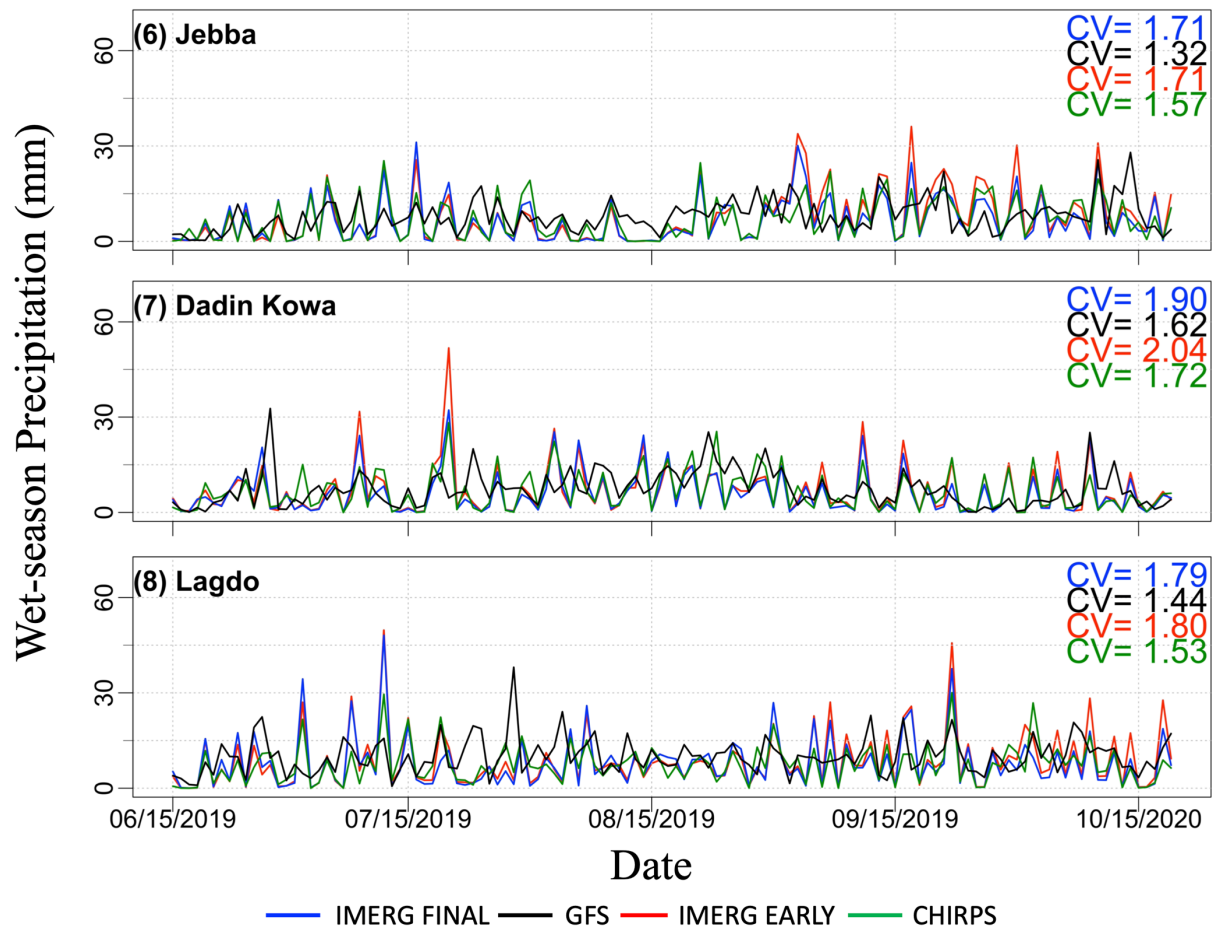
Figure 6. Same as in Figure 5 but for the remaining three watersheds.

Figure 7 displays the performance statistics of watershed-averaged daily rainfall (validated against IMERG Final) in terms of Kling-Gupta Efficiency (KGE), Bias Ratio (BR), correlation (R), variability ratio (γ), and root mean square error normalized by reference precipitation mean (NRMSE). First, the performance results for the 1-day lead GFS are considered. The KGE scores are poor (0.3 < KGE < 0.5) for half of the watersheds considered (Selingue, Goronyo, Bakolori, and Lagdo) and intermediate (0.5 < KGE < 0.75) for the remaining half watersheds (Markala, Kainji, Jebba, and Dadin Kowa). The breakdown of the KGE scores (BR, R, and γ) reveals the key factors contributing to the KGE estimates. The GFS tends to overestimate daily precipitation for most sub-basins, as BR is higher than one, except for Kainji. The overestimation is particularly high for Selingue and Markala, where BR is 1.33 and 1.22, respectively. The correlation coefficient between GFS and IMERG Final is mostly low (R < 0.60), and is particularly lower for Bakolori (R=0.36) and Goronyo (R=0.43). The variability ratio of GFS is mostly between 0.69 to 0.83 (except for

318   Kainji, where γ is 1.09), indicating that the GFS tends to give lower temporal variability of rainfall. The NRMSE is

319   very high, ranging from 100% to 266%, and is particularly high for Goronyo (266%) and Bakolori (264%), which are

320   relatively small-sized watersheds.

321

322   Next, the performance of IMERG Early was examined with respect to IMERG Final, mainly to assess if it is possible

323   to use the near-real-time IMERG Early product to calibrate and improve the accuracy of GFS forecasts. The IMERG

324   Early performs much better with KGE values higher than 0.75 (except for Kainji where KGE is 0.69), correlation

325   higher than 0.90, and variability ratio close to the optimum value. The high performance of IMERG Early is due to its

326   similarity with the IMERG Final product, as the main difference between the two products is that IMERG Early,

327   unlike IMERG Final, does not use monthly rain gauge observations for bias correction. Such monthly bias correction

328   techniques would not alter the pattern and variability of IMERG Early compared to IMERG Final. Therefore, the

329   performance of IMERG Early should be evaluated using bias statistics, the other statistics (correlation and variability

330   ratio) are presented for completeness. IMERG Early overestimates rainfall in most watersheds in the range 11%

331   (Lagdo) to 28% (Kainji) except for two watersheds, where it slightly underestimates by 14% (Selingue) and 11%

332   (Markala). Comparison of the performance of GFS and IMERG Early indicates that both products have different bias

333   characteristics. In some watersheds (e.g., Kainji), GFS outperforms IMERG Early in terms of bias, whereas in other

334   watersheds (e.g., Markala), IMERG Early outperforms GFS.

335

336   CHIRPS was also compared with IMERG Final to assess how the use of different reference products may affect the

337   finding about the performance of GFS forecasts. The KGE scores of CHIRPS are higher than 0.75 in all cases,

338   indicating that CHIRPS and IMERG Final have comparable KGE performance. Therefore, the performance of GFS

339   is expected to be about the same even if the reference product used this in this study (IMERG Final) changes to

340   CHIRPS.

341

342

343

344

345

346
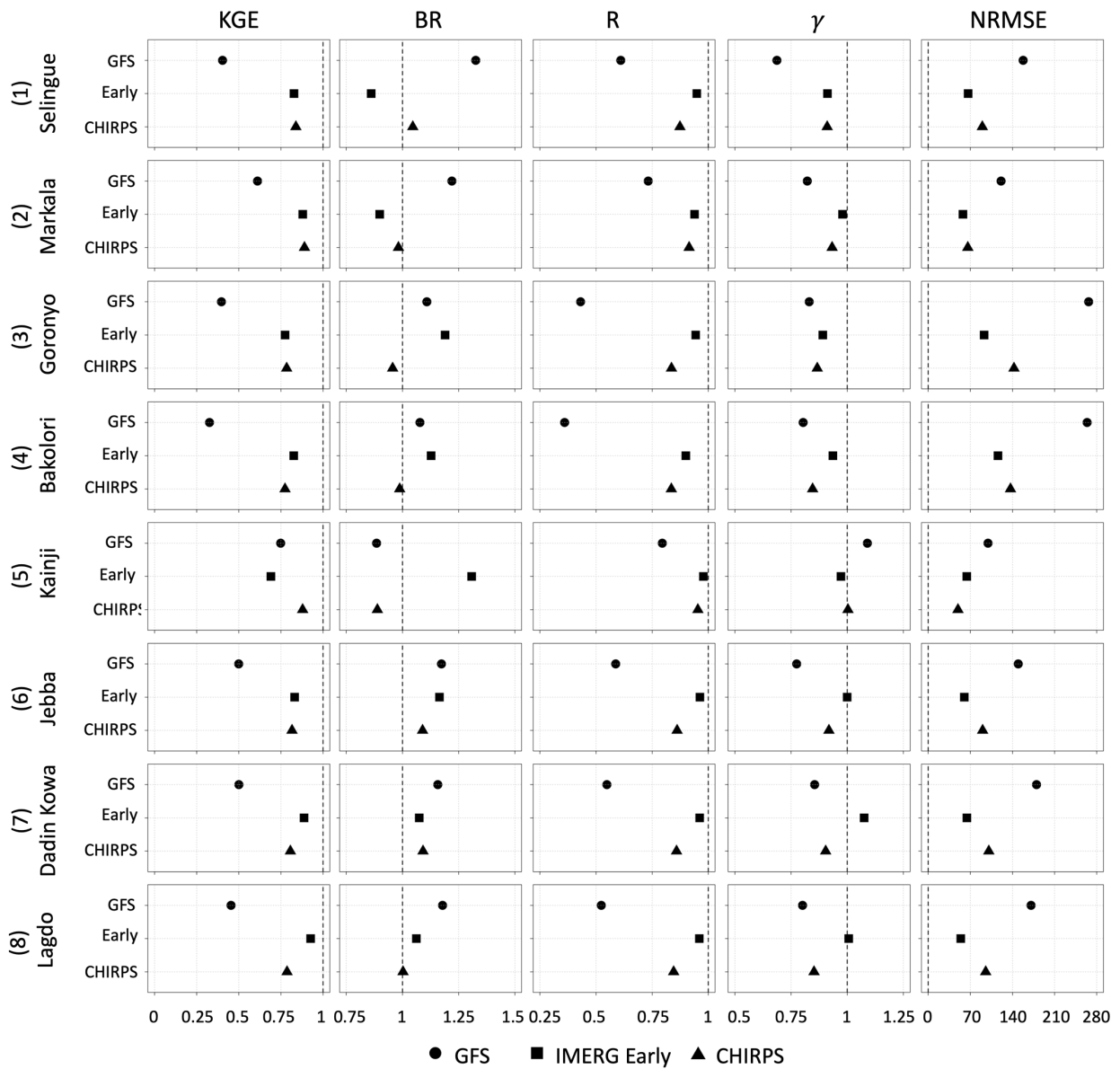
Figure 7. Summary of performance statistics (Kling-Gupta Efficiency KGE, Bias Ratio BR, correlation R, variability ratio γ, and root mean square error normalized by reference rainfall [%], for the 1-day lead time GFS forecasts and other satellite products. The time period considered was June 15, 2019 – June 15, 2020.
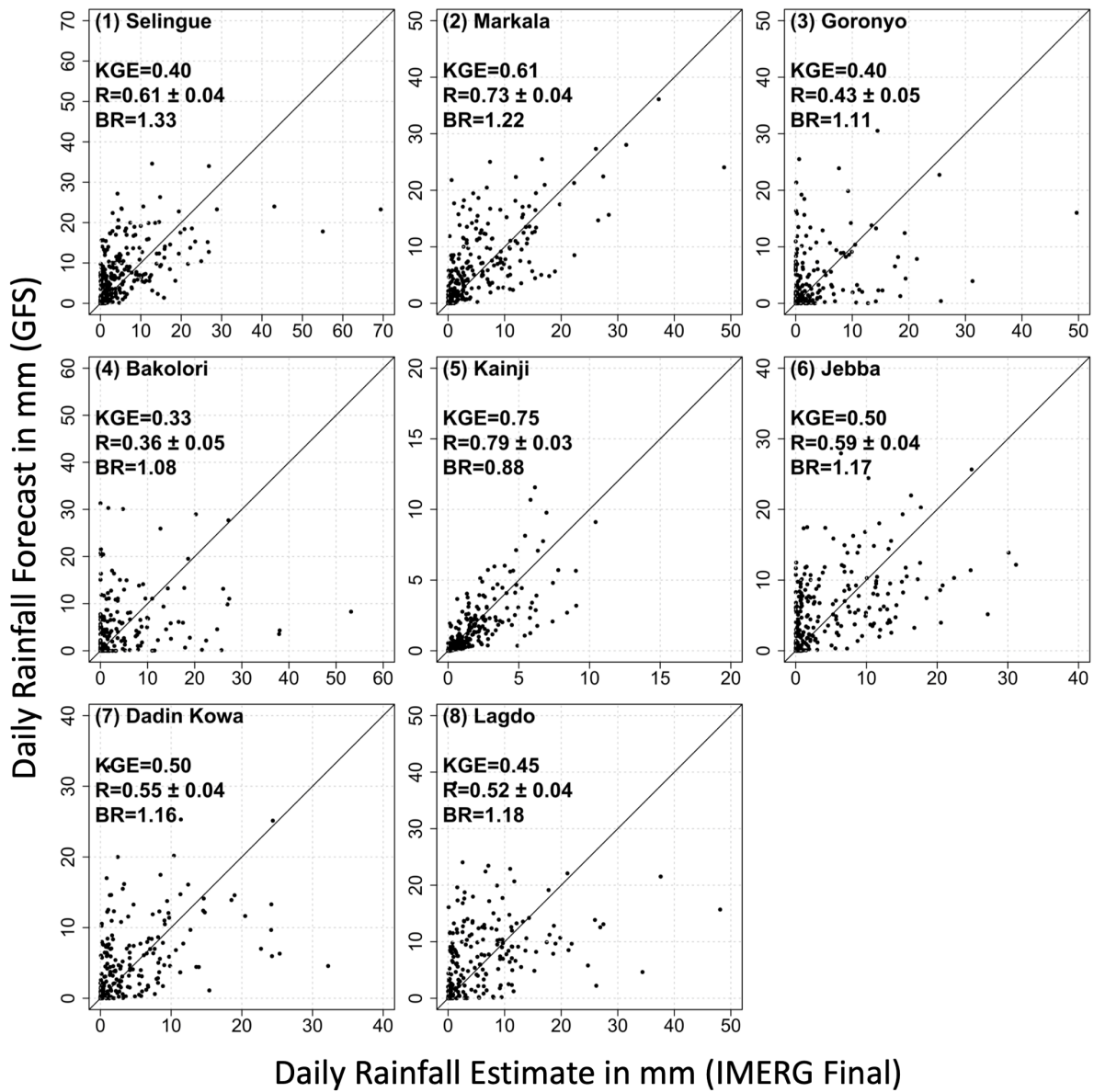
347

348

349

350

351

352

353

354

Figure 8. Scatterplot of watershed-averaged daily precipitation forecast obtained from 1-day lead GFS forecasts against corresponding values from IMERG Final.

3.4 Dependence of Forecast Performance on Precipitation Rate

Figure 8 presents the scatterplot of 1-day lead GFS forecasts and IMERG Final at daily and watershed-average scales.

The performance of GFS varies between watersheds. In the Markala and Kainji watersheds, GFS forecasts agree well

with IMERG Final at almost all rain rates. In the Selingue watershed, GFS agrees well with IMERG Final for rain

rates under 30 mm/day, but GFS substantially underestimates all rain rates above 30 mm/day. In the remaining five

19

watersheds, GFS has poor performance, replete with large scatter, high false alarm, and large underestimation bias of heavy rain rates.

**3.5 Dependence of Daily Forecast Performance on Lead Time and Spatial Scale**

In order to assess the effect of various lead times and spatial scales on forecast performance, we obtained daily GFS forecasts at various lead times (1-day, 5-day, 10-day, and 15-day), and aggregated the forecasts at spatial scales from 0.25° to coarser scales (0.5°, 0.75°, and 1°) by averaging grids. The purpose of degrading the resolution is to determine at which resolution the forecasts have acceptable performance. The KGE value at each spatial resolution was calculated in the following steps: (i) average the data at the required spatial resolution, (ii) extract pairs of data (one from IMERG Final, and the other from GFS), (iii) concatenate the pairs to form one large series of data, and (4) compute a single KGE from this data series. The resulting KGE values are shown in Fig. 9.

With regard to the effect of spatial scales, the KGE at the GFS native resolution (i.e. 0.25°) is very low. As the spatial scale increases, KGE increases, as expected. For instance, for Markala watershed KGE increases from 0.27 (0.25°) to 0.40 (1°) for a 1-day lead. This indicates that the variation in KGE values between the watersheds could be partly explained by the watershed size. For example, based on Fig. 5, the KGE for the 1-day lead daily GFS forecast was the highest for the largest Kainji watershed (watershed area of 1,464,092 Km^2) and the lowest for the smallest Bakolori watershed (4,887 Km^2). With regard to the effect of lead time for daily forecasts, KGE decreases significantly as lead time increases. For instance, for Markala watershed and a grid size of 1°, KGE decreases from 0.40 (1-day lead) to 0.21 (15-day lead).

383
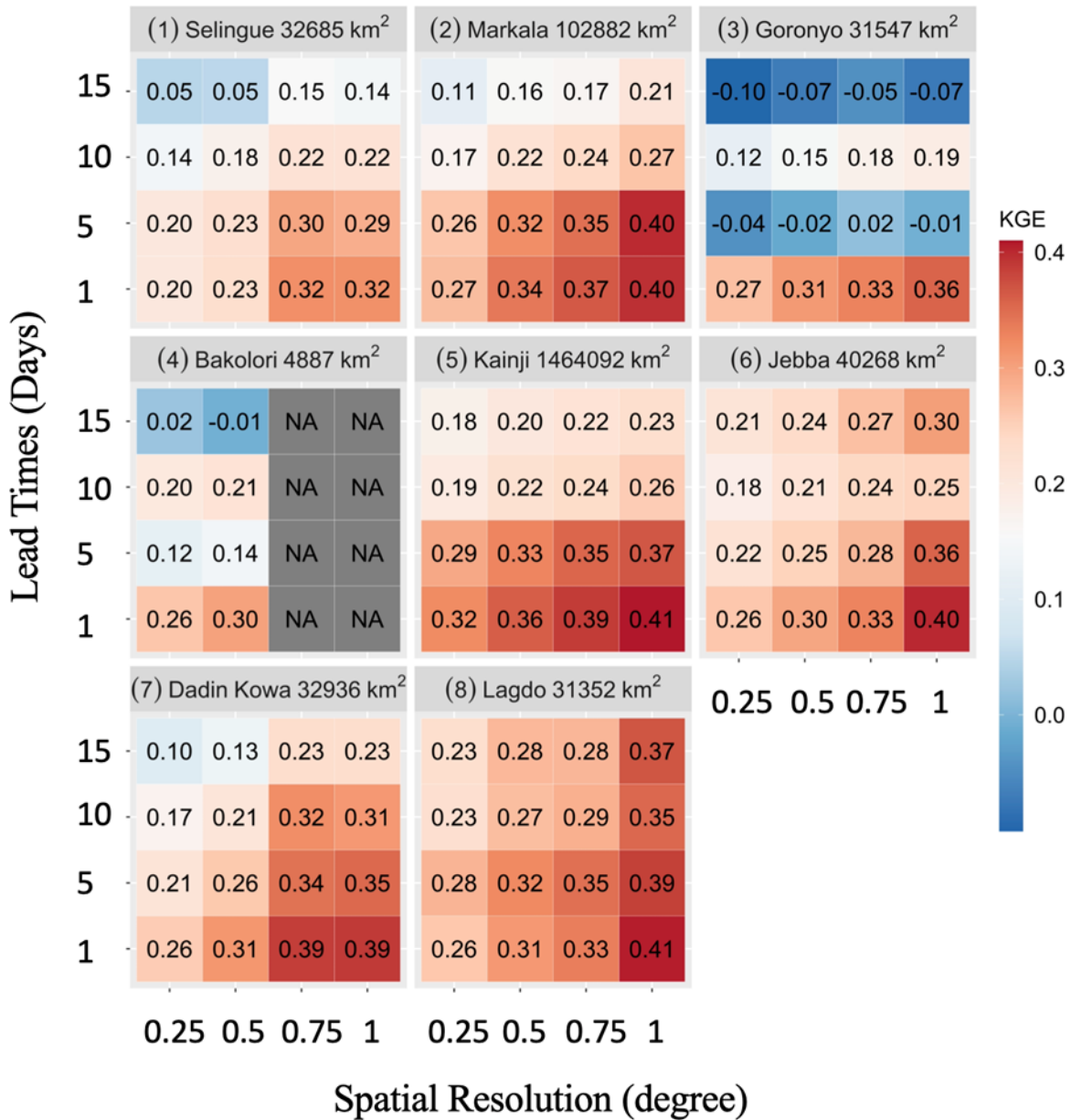
384
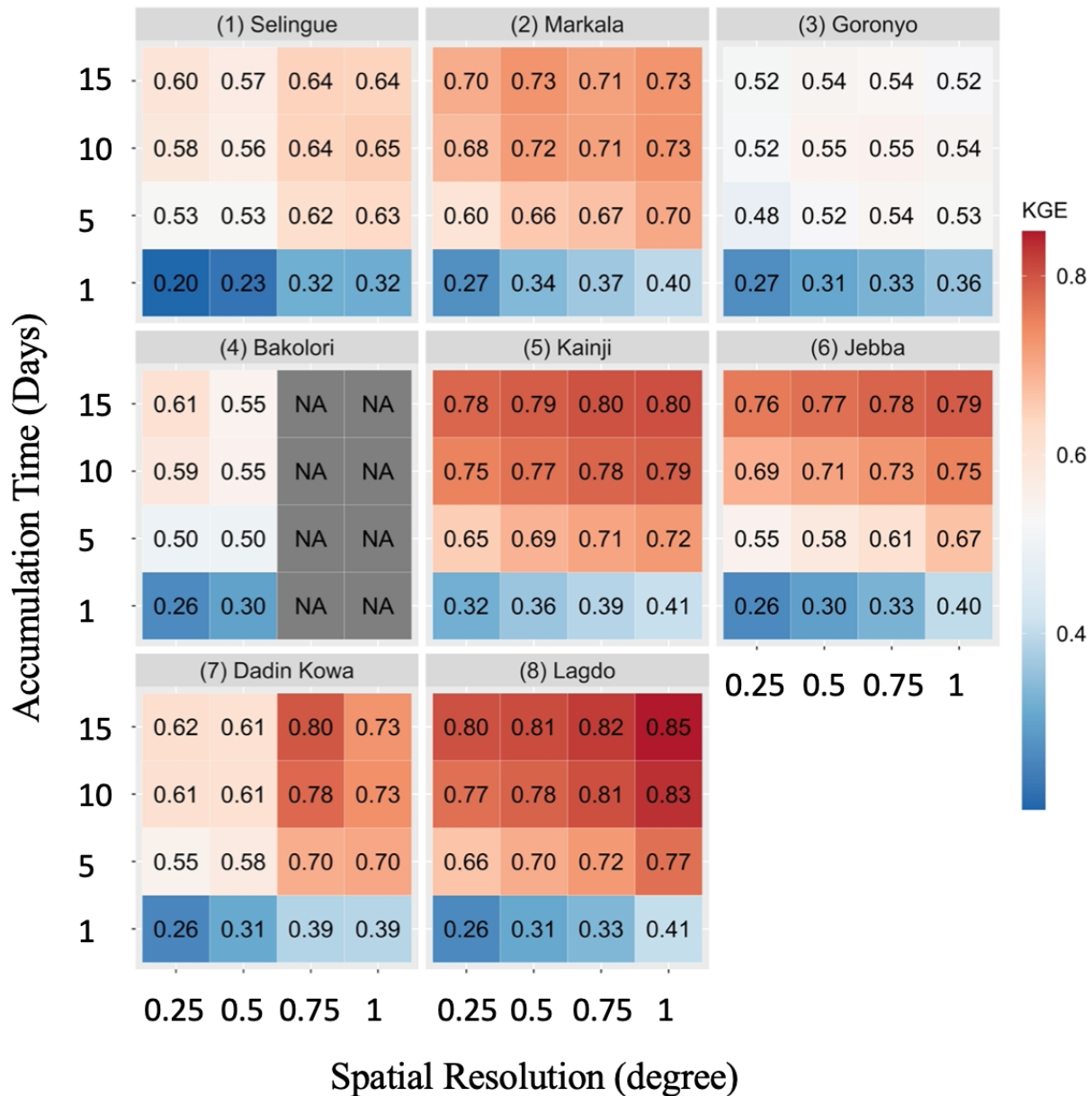385 Figure 9. Kling-Gupta Efficiency (KGE) for daily precipitation of GFS as a function of lead time (1-day, 5-
386 day, and 15-day) and spatial scale (0.25°, 0.50°, 0.75°, 1.0°). The dam names and corresponding watershed areas are
387 given in the titles.
388

### 3.6 Effect of Temporal Aggregation Scale on Forecast Performance

389

390 To assess the effect of temporal aggregation scale, we obtained the 1-day total, 5-day total, 10-day total, and 15-day

391 total GFS precipitation forecasts. These multi-day forecasts are constructed by combining multiple lead-time forecasts.

392 For instance, the 5-day total forecast is obtained by adding the 1-day lead, 2-day lead, 3-day lead, 4-day lead, and 5-

21

day lead daily forecasts. Figure 10 presents the KGE values for GFS forecasts over different temporal aggregation scales, and different grid sizes. Temporal aggregation substantially increases KGE at all spatial scales. For example, at the grid size of 1° over Markala watershed, the KGE values jump from 0.40 at daily timescale to 0.73 at 15-day total timescale.


Figure 10. Kling-Gupta Efficiency (KGE) of GFS as a function of accumulation time scale (1-day, 5-day, 10-day, and 15-day) and spatial scale (0.25°, 0.50°, 0.75°, 1.0°).

400   In Figure 11, we show the performance statistics of GFS for 15-day accumulated watershed-averaged rainfall forecast.

401   The KGE values are intermediate (0.5 < KGE < 0.75) for four watersheds and good (KGE > 0.75) for the remaining

402   four watersheds. Analysis of the components of KGE reveals that the improvement of KGE at longer timescales comes

403   as a result of improved correlation and variability ratio. At the 15-day accumulation timescale, IMERG Early estimates

404   have less bias than GFS at all watersheds, except at Kainji watershed. Figure 12 presents the scatterplot of 15-day

405   accumulated GFS forecast vs IMERG Final. In general, the GFS estimates perform well for low to moderate rain rates,

406   but tend to overestimate higher rain rates. This is consistent with Wang et al. (2019) who reported the difficulty of

407   capturing the magnitude of high rain rates in GFS model.
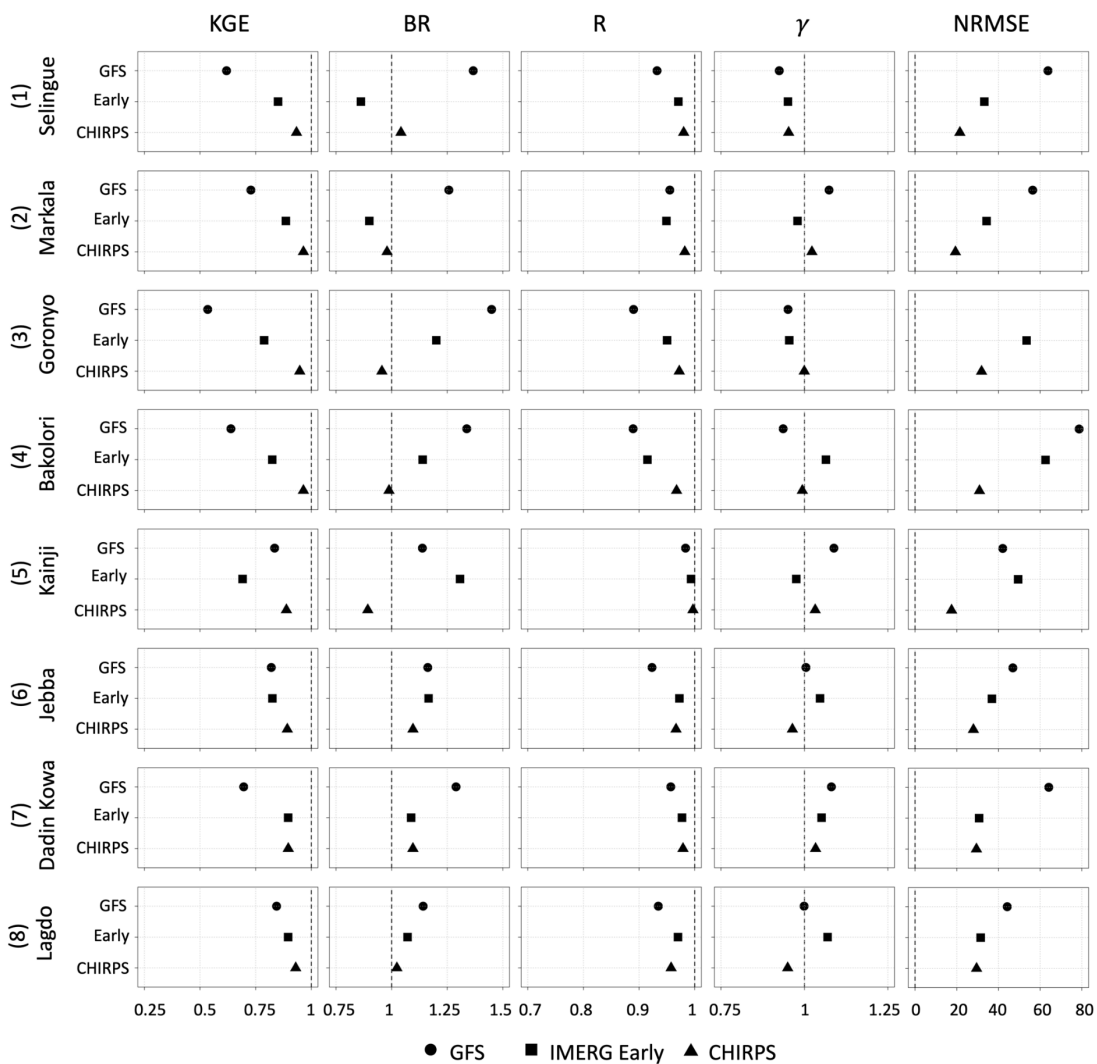
Figure 11. Summary of performance statistics (Kling-Gupta Efficiency KGE, Bias Ratio BR, correlation R, variability ratio γ, and root mean square error normalized by reference rainfall [%], for the 15-day accumulated GFS forecast and other satellite products.
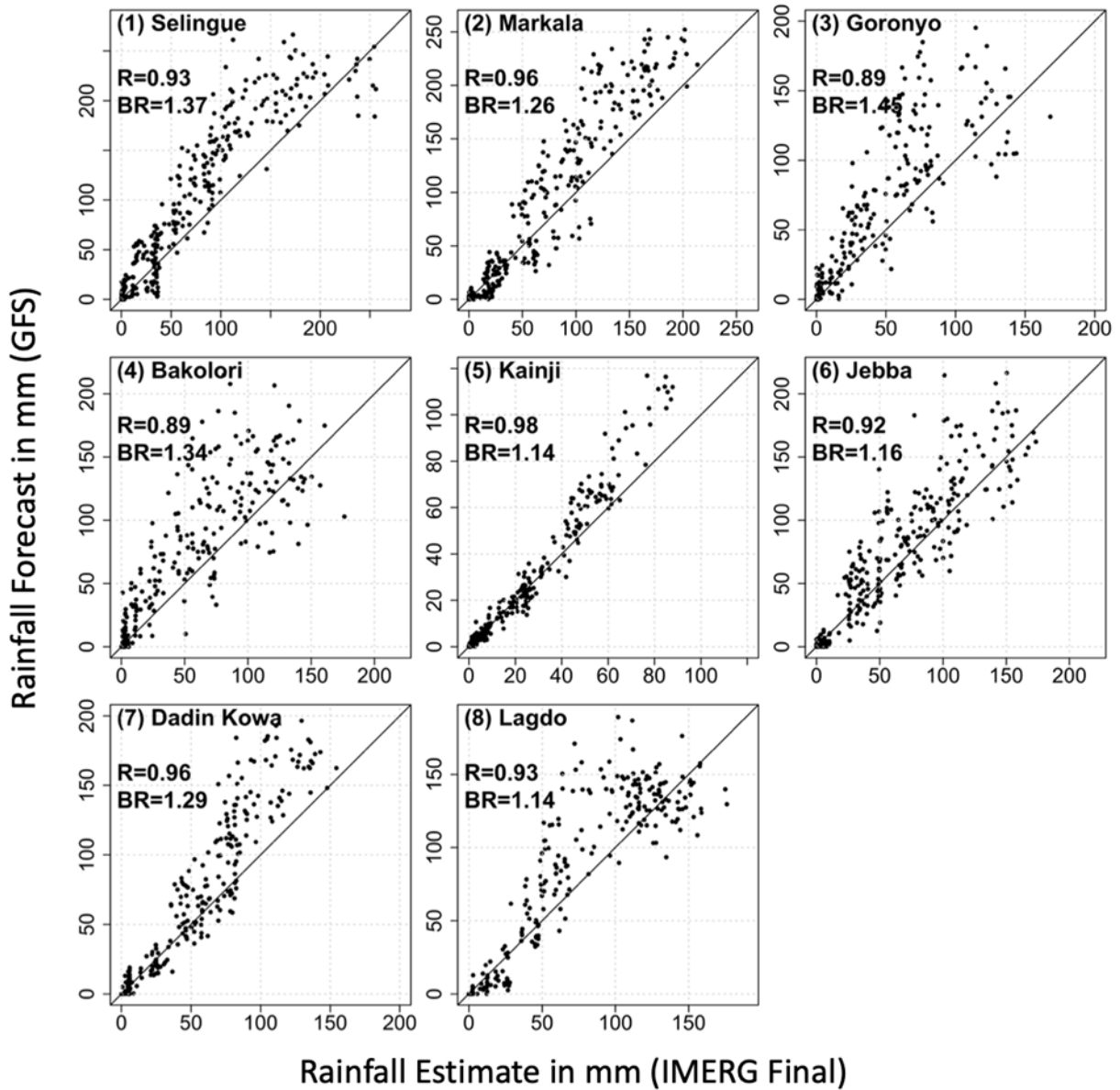
Figure 12. Scatterplot of watershed-averaged 15-day accumulated precipitation forecast obtained from GFS forecast against corresponding values from IMERG Final.

4. Conclusions

This study has evaluated the accuracy of medium-range (1-day to 15-day lead time) forecasts available from the Global Forecast System (GFS), for the watersheds of large dams in the Niger river basin. Despite the limited temporal coverage, some consistent features emerged from this evaluation. The accuracy of GFS forecast depends on climatic regime, lead time, accumulation timescale, and spatial scale. With regard to the role of climatic regimes, the GFS

421   forecast has large overestimation bias in the Guinea (wet climatic regime), moderate overestimation bias in the

422   Savannah (moderately wet climatic regime), but has no bias in the Sahel (dry climate). With regard to lead time, as

423   the lead time increases, the forecast accuracy decreases. Averaging the forecasts at coarser spatial scales leads to

424   increased forecast accuracy. For daily rainfall forecasts, the performance of GFS is very low (KGE < 0.32) at almost

425   all watersheds except at Markala (KGE = 0.44) and Kainji (KGE = 0.68), both of which have much larger watershed

426   areas compared to the other watersheds. Averaging the forecasts at longer time scales also leads to increased forecast

427   accuracy. For 15-day rainfall accumulation timescale, the KGE values are either "intermediate" (i.e., $0.50 \leq KGE \leq$

428   0.75) for half of the watersheds (Selingue, Goronyo, Bakolori, and Daddin Kowa) or "good" (i.e., $KGE \geq 0.75$) for

429   the remaining half (Markaa, Kainji, Jebba, and Lagdo). With regard to the effect of rainfall rate, the 15-day

430   accumulated GFS forecasts tend to perform better for low to medium rain rates, but contain large overestimation bias

431   at high rain rates.

432

433   The performance statistics of GFS indicate the need for calibrating GFS forecasts in order to improve their accuracy.

434   Post-processing calibration of GFS forecasts requires the use of "relatively better performing" and "available in near-

435   real-time" independent rainfall observations to correct real-time dynamical GFS model forecasts. This study has

436   compared the performance of IMERG Early satellite rainfall products with the performance of GFS in terms of bias.

437   In the Guinea and Savannah regions, IMERG Early outperforms GFS in terms of bias, while in the dry Sahel region,

438   IMERG Early is outperformed by GFS.

439

440   We acknowledge that the reference dataset used in our evaluation (i.e., IMERG Final) has its own estimation errors.

441   We conducted additional assessment to evaluate the performance of IMERG Final with respect to another independent

442   and high-quality (i.e. satellite-gauge merged) rainfall product (i.e. CHIRPS). Our results show that IMERG Final and

443   CHIRPS have similar rainfall characteristics, indicating the robustness of IMERG Final.

444

445   Overall, we conclude that the GFS forecasts, at 15-day accumulation timescale, have acceptable performance,

446   although they tend to overestimate high rain rates. The shorter the time scale, the lower is the GFS performance. Given

447   that IMERG Early outperforms GFS particularly in the wet region of the Niger, we recommend testing the suitability

448   of IMERG Early to serve as input into post-processing of GFS in order to improve the accuracy of GFS forecasts.

449   Possible post-processing techniques that could be explored include: simple bias (multiplicative) correction

450   (Gumindoga et al. 2019), multi-resolution bias correction through wavelet analysis (Xu et al. 2019) or empirical mode

451   decomposition method (Wang et al. 2020, Prasad et al. 2019), and Artificial Intelligence-based methods such as Feed

452   Forward Neural Network (Cloud et al. 2019), Support Vector Machine ((Du et al. 2017; Yu et al. 2017), and Adaptive

453   Neural Fuzzy Inference System (Jehanzaib et al. 2021).

454

455

456

457

458

459

460

461

462

463

464

465

466

467

468

469

470

471

472

473

474

475

476

477

478

5. Data and Code Availability

We acknowledge the National Center for Atmospheric Research (NCAR) for providing public access to the GFS rainfall forecast data products (https://rda.ucar.edu/datasets/ds084.1/), NASA for providing public access to IMERG Final and IMERG Early rainfall data products (https://disc.gsfc.nasa.gov), and the University of California Santa Barbara's (UCSB) Climate Hazard's group for providing public access to CHIRPS rainfall data (https://www.chc.ucsb.edu/data).

485

486

6. Author Contribution

H. Yue: data processing, data analysis, and manuscript preparation; M. Gebremichael: project oversight, method design, contribution to manuscript text; V. Nourani: method design, contribution to manuscript text.

490

491

7. Competing Interests

The authors declare that they have no conflict of interest.

494

495

498

499   **References**

500   Abdalla, S., Janssen, P. A., Balmaseda, M. A., Mogensen, K., Bidlot, J. R., & Keeley, S.: ECMWF Experience In
501   Global Monitoring And Validation Of Radar Altimetry Products. In ESA Living Planet Symposium 2013, 9-13 Sep.
502   2013, Edinburgh, ESA Proceedings No. SP-722 (CD), 2013 December

503   Akinsanola, A. A., and Zhou, W.: Projections of West African summer monsoon rainfall extremes from two CORDEX
504   models. Climate Dynamics, 52(3), 2017-2028, doi:10.1007/s00382-018-4238-8, 2018

505   Akinsanola, A. A., Ogunjobi, K. O., Gbode, I. E., and Ajayi, V. O.: Assessing the capabilities of three regional climate
506   models over CORDEX Africa in simulating West African summer monsoon precipitation. Advances in Meteorology,
507   doi:10.1155/2015/935431, 2015.

508   Akinsanola, A.A., Ajayi, V.O., Adejare, A.T., Adeyeri, O.E., Gbode, I.E., Ogunjobi, K.O., Nikulin, G. and Abolude,
509   A.T.: Evaluation of rainfall simulations over West Africa in dynamically downscaled CMIP5 global circulation
510   models. Theoretical and applied climatology., 132(1), 437-450, doi:10.1007/s00704-017-2087-8, 2017.

511   Alexander, S., Yang, G., Addisu, G., and Block, P.: Forecast-informed reservoir operations to guide hydropower and
512   agriculture allocations in the Blue Nile basin, Ethiopia. International Journal of Water Resources Development, 1-26,
513   doi:10.1080/07900627.2020.1745159, 2020

514   Alfieri, L., Burek, P., Dutra, E., Krzeminski, B., Muraro, D., Thielen, J., and Pappenberger, F.: GloFAS–global
515   ensemble streamflow forecasting and flood early warning. Hydrology and Earth System Sciences, 17(3), 1161-1175,
516   doi:10.5194/hess-17-1161-2013, 2013

517   Animashaun, I. M., Oguntunde, P. G., Akinwumiju, A. S., and Olubanjo, O. O.: Rainfall Analysis over the Niger
518   Central Hydrological Area, Nigeria: Variability, Trend, and Change point detection. Scientific African, 8, e00419,
519   doi: 10.1016/j.sciaf.2020.e00419, 2020

520   Arakawa, A., and Schubert, W. H.: Interaction of a cumulus cloud ensemble with the large-scale environment, Part I.
521   Journal of the Atmospheric Sciences, 31(3), 674-701, 1974.

522   Bhuiyan, M.A., Nikolopoulos. E.I., and Anagnostou, E.N.: Machine Learning-Based Blending of Satellite and
523   Reanalysis Precipitation Datasets: A Multiregional Tropical Complex Terrain Evaluation, Journal of
524   Hydrometeorology, 20(11), 2147-2161, doi: 10.1175/JHM-D-19-0073.1, 2019.

525   Bliefernicht, J., Waongo, M., Salack, S., Seidel, J., Laux, P., and Kunstmann, H.: Quality and value of seasonal
526   precipitation forecasts issued by the West African regional climate outlook forum. Journal of Applied Meteorology
527   and Climatology, 58(3), 621-642, doi:10.1175/JAMC-D-18-0066.1, 2019.

528   Breuer, N. E., Fraisse, C.W., and Cabrera, V.E.: The Cooperative Extension Service as a boundary organization for
529   diffusion of climate forecasts: A 5-year study. Journal of Extension, 48(4), 2010, Article Number 4RIB7, 5 pp.

530   Chen, F., Janjić, Z., and Mitchell, K. Impact of atmospheric surface-layer parameterizations in the new land-surface
531   scheme of the NCEP mesoscale Eta model. Boundary-Layer Meteorology, 85(3), 391-421, doi:
532   10.1023/A:1000531001463, 1997.

533   Cloud, K. A., Reich, B. J., Rozoff, C. M., Alessandrini, S., Lewis, W. E., & Delle Monache, L.: A feed forward neural
534   network based on model output statistics for short-term hurricane intensity prediction. Weather and
535   Forecasting, 34(4), 985-997, doi: 10.1175/WAF-D-18-0173.1, 2019.

536   Clough, S., Shephard, M., Mlawer, E., Delamere, J., Iacono, M., Cady-Pereira, K., Boukabara, S., and Brown, P.:
537   Atmospheric radiative transfer MODELING: A summary of the AER codes. Journal of Quantitative Spectroscopy
538   and Radiative Transfer, 91(2), 233-244. doi:10.1016/j.jqsrt.2004.05.058, 2005.

539   Dembélé, M., Schaefli, B., van de Giesen, N., and Mariéthoz, G.: Suitability of 17 rainfall and temperature gridded
540   datasets for largescale hydrological modelling in West Africa. Hydrol. Earth Syst. Sci. Discuss., https://doi.
541   org/10.5194/hess-2020-68, in review, 2020

542   Dezfuli, A. K., Ichoku, C. M., Huffman, G. J., Mohr, K. I., Selker, J. S., Van De Giesen, N., Hochreutener, R., and
543   Annor, F. O.: Validation of IMERG precipitation in Africa. Journal of hydrometeorology, 18(10), 2817-2825, doi:
544   10.1175/JHM-D-17-0139.1, 2017a

28

545 Dezfuli, A. K., Ichoku, C. M., Mohr, K. I., & Huffman, G. J.: Precipitation characteristics in West and East Africa
546 from satellite and in situ observations. Journal of Hydrometeorology, 18(6), 1799-1805, doi:10.1175/JHM-D-17-
547 0068.1, 2017b

548 Du, J., Liu, Y., Yu, Y., & Yan, W.: A prediction of precipitation data based on support vector machine and particle
549 swarm optimization (PSO-SVM) algorithms. Algorithms, 10(2), 57, doi: 10.3390/a10020057, 2017

550 Funk, C., Peterson, P., Landsfeld, M., Pedreros, D., Verdin, J., Shukla, S., Husak, G., Rowland, J., Harrison, L., Hoell,
551 A., and Michaelsen, J.: The climate hazards infrared precipitation with stations—a new environmental record for
552 monitoring extremes. Scientific data, 2(1), 1-21, doi:10.1038/sdata.2015.66, 2015.

553 Gossett, M., Alcoba, M., Roca, R., Cloche, S., and Urbani, G.: Evaluation of TAPEER daily estimates and other GPM-
554 era products against dense gauge networks in West Africa, analysing ground reference uncertainty. 144(1), 255-269,
555 doi: 10.1002/qj.3335, 2018.

556 Grell, G. A.: Prognostic evaluation of assumptions used by cumulus parameterizations. Monthly weather review,
557 121(3), 764-787, doi: 10.1175/1520-0493(1993)121<0764:PEOAUB>2.0.CO;2, 1993.

558 Gumindoga, W., Rientjes, T. H., Haile, A. T., Makurira, H., & Reggiani, P.: Performance of bias-correction schemes
559 for CMORPH rainfall estimates in the Zambezi River basin. Hydrology and earth system sciences, 23(7), 2915-2938,
560 doi: 10.5194/hess-23-2915-2019, 2019.

561 Gupta, H. V., Kling, H., Yilmaz, K. K., and Martinez, G. F.: Decomposition of the mean squared error and NSE
562 performance criteria: Implications for improving hydrological modelling. Journal of hydrology, 377(1-2), 80-91, doi:
563 10.1016/j.jhydrol.2009.08.003, 2009.

564 Haile, A. T., Tefera, F. T., and Rientjes, T.: Flood forecasting in Niger-Benue basin using satellite and quantitative
565 precipitation forecast data. International journal of applied earth observation and geoinformation, 52, 475-484, doi:
566 10.1016/j.jag.2016.06.021, 2016.

567 Hou, A. Y., Kakar, R. K., Neeck, S., Azarbarzin, A. A., Kummerow, C. D., Kojima, M., Oki, R., Nakamura, K., and
568 Iguchi, T.: The global precipitation measurement mission. Bulletin of the American Meteorological Society, 95(5),
569 701-722, doi:10.1175/BAMS-D-13-00164.1, 2014.

570 Huffman, G. J., Adler, R., Bolvin, D., and E. Nelkin, E.: The TRMM Multi-Satellite Precipitation Analysis (TMPA).
571 Satellite Rainfall Applications for Surface Hydrology, M. Gebremichael and F. Hossain, Eds., Springer, 3–22, 2010.

572 Huffman, G. J., Bolvin, D. T., Braithwaite, D., Hsu, K., Joyce, R., Xie, P., & Yoo, S. H.: NASA global precipitation
573 measurement (GPM) integrated multi-satellite retrievals for GPM (IMERG). Algorithm Theoretical Basis Document
574 (ATBD) Version, 4, 26, 2015.

575 Huffman, G. J., Bolvin, D. T., Nelkin, E. J., Wolff, D. B., Adler, R. F., Gu, G., Hong, Y., Bowman, K.P. and Stocker,
576 E. F.: The TRMM Multisatellite Precipitation Analysis (TMPA): Quasi-Global, Multiyear, Combined-Sensor
577 Precipitation estimates at fine scales. Journal of Hydrometeorology, 8(1), 38-55. doi:10.1175/jhm560.1, 2007.

578 Huffman, G.J., Stocker, E.F., Bolvin, D.T., Nelkin, E.J., Jackson J.: GPM IMERG Final Precipitation L3 1 day 0.1
579 degree x 0.1 degree V06, Edited by Andrey Savtchenko, Greenbelt, MD, Goddard Earth Sciences Data and
580 Information Services Center (GES DISC), Accessed: [Feb 11, 2021], doi:10.5067/GPM/IMERGDF/DAY/06, 2019a

581 Huffman, G.J., Stocker, E.F., Bolvin, D.T., Nelkin, E.J., Jackson J.: GPM IMERG Early Precipitation L3 1 day 0.1
582 degree x 0.1 degree V06, Edited by Andrey Savtchenko, Greenbelt, MD, Goddard Earth Sciences Data and
583 Information Services Center (GES DISC), Accessed: [Feb 11, 2021], doi:10.5067/GPM/IMERGDE/DAY/06, 2019b

584 Iacono, M. J., Mlawer, E. J., Clough, S. A., and Morcrette, J. J.: Impact of an improved longwave radiation model,
585 RRTM, on the energy budget and thermodynamic properties of the NCAR community climate model, CCM3. Journal
586 of Geophysical Research: Atmospheres, 105(D11), 14873-14890, doi: 10.1029/2000JD900091, 2000.

587 Jehanzaib, M., Bilal Idrees, M., Kim, D., & Kim, T. W.: Comprehensive Evaluation of Machine Learning Techniques
588 for Hydrological Drought Forecasting. Journal of Irrigation and Drainage Engineering, 147(7), 04021022, doi:
589 10.1061/(ASCE)IR.1943-4774.0001575, 2021

590 Jiang, M., Feng, J., Li, Z., Sun, R., Hou, Y. T., Zhu, Y., Wan, B., Guo, J., and Cribb, M.: Potential influences of
591 neglecting aerosol effects on the NCEP GFS precipitation forecast. Atmospheric Chemistry and Physics, 17(22),
592 13967–13982, doi: 10.5194/acp-17-13967-2017, 2017.

593 JMA.: Outline of the operational numerical weather prediction at the Japan Meteorological Agency (Appendix to
594 WMO numerical weather prediction progress report). Japan Meteorological Agency, 47pp. (available online
595 at https://www.jma.go.jp/jma/jma-eng/jma-center/nwp/outline2019-nwp/index.htm; last accessed: February 2021),
596 2019.

597 Kling, H., Fuchs, M., and Paulin, M.: Runoff conditions in the upper Danube basin under an ensemble of climate
598 change scenarios. Journal of Hydrology, 424, 264-277, 2012.

599 Koppa, A., Gebremichael, M., Zambon, R.C., Yeh, W.W.G., and Hopson, T.M.: Seasonal Hydropower Planning for
600 Data-Scarce Regions Using Multimodel Ensemble Forecasts, Remote Sensing Data, and Stochastic Programming.
601 WATER RESOURCES RESEARCH, 55(11), 8583-8607, DOI: 10.1029/2019WR025228, 2019.

602 Lehner, B., and 14 coauthors: High-resolution mapping of the world's reservoirs and dams for sustainable river-flow
603 management. Frontiers in Ecology and the Environment 9 (9): 494-502, 2011

604 Lehner, B., Verdin, K., Jarvis, A.: New global hydrography derived from spaceborne elevation data. Eos, Transactions,
605 AGU, 89(10): 93-94, 2008

606 Lien, G. Y., Kalnay, E., Miyoshi, T., and Huffman, G. J.: Statistical properties of global precipitation in the NCEP
607 GFS model and TMPA observations for data assimilation. Monthly Weather Review, 144(2), 663–679, doi:
608 10.1175/MWR-D-15-0150.1, 2016.

609 Maranan, M., Fink, A. H., Knippertz, P., Amekudzi, L. K., Atiah, W. A., and Stengel, M.: A process-based validation
610 of GPM IMERG and its sources using a mesoscale rain gauge network in the West African forest zone. Journal of
611 Hydrometeorology, 21(4), 729-749, 2020

612 Mase, A. S., and Prokopy, L.S.: Unrealized Potential: A review of perceptions and use of weather and climate infor-
613 mation in agricultural decision making. Weather Climate and Society 6(1):47-61. DOI: 10.1175/Wcas-D-12-00062.1,
614 2014.

615 Mlawer, E. J., Taubman, S. J., Brown, P. D., Iacono, M. J., and Clough, S. A.: Radiative transfer for inhomogeneous
616 atmospheres: RRTM, a validated correlated-k model for the longwave. Journal of Geophysical Research:
617 Atmospheres, 102(D14), 16663-16682, 1997.

618 National Centers for Environmental Prediction.: National Centers for Environmental Prediction: The Global Forecast
619 System (GFS) -Global Spectral Model (GSM). Retrieved from
620 https://www.emc.ncep.noaa.gov/emc/pages/numerical_forecast_systems/gfs/documentation.php, last access: Sep
621 2021, 2021a

622 National Centers for Environmental Prediction.: National Centers for Environmental Prediction: FV3: The GFDL
623 Finite-Volume Cubed-Sphere Dynamical Core, Retrieved from https://www.gfdl.noaa.gov/fv3/, last access: Sep 2021,
624 2021b

625 National Centers for Environmental Prediction/National Weather Service/NOAA/U.S. Department of Commerce.:
626 NCEP GFS 0.25 Degree Global Forecast Grids Historical Archive, doi:10.5065/D65D8PW, 2015

627 Pandya, R., Hodgson, A., Hayden, M.H., Akweongo, P., Hopson, T., Forgor, A.A., Yoksas, T., Dalaba, M.A., Dukic,
628 V., Mera, R., and Dumont, A., McCormack, K., Anaseba, D., Awine, T., Boehnert, J., Nyaaba, G., Laing, A., and
629 Semazzi, F.: Using weather forecasts to help manage meningitis in the West African Sahel. Bulletin of the American
630 Meteorological Society 96(1):103-+. doi: 10.1175/Bams-D-13-00121.1, 2015

631 Patt, A. G., Ogallo, L., and Hellmuth, M.: Sustainability—Learning from 10 years of climate outlook forums in Africa.
632 Science 318(5847):49-50. doi:10.1126/science.1147909, 2007.

633 Pirret, J. S., Daron, J. D., Bett, P. E., Fournier, N., and Foamouhoue, A. K.: Assessing the skill and reliability of
634 seasonal climate forecasts in Sahelian West Africa. Weather and Forecasting, 35(3), 1035-1050, doi:10.1175/WAF-
635 D-19-0168.1, 2020.

636 Prasad, R., Deo, R. C., Li, Y., & Maraseni, T.: Weekly soil moisture forecasting with multivariate sequential, ensemble
637 empirical mode decomposition and Boruta-random forest hybridizer algorithm approach. Catena, 177, 149-166, doi:
638 10.1016/j.catena.2019.02.012, 2019.

639   Roudier, P., Alhassane, A., Baron, C., Louvet, S., and Sultan, B.: Assessing the benefits of weather and seasonal
640   forecasts to millet growers in Niger. Agricultural and forest meteorology, 223, 168-180, doi:
641   10.1016/j.agrformet.2016.04.010, 2016.

642   Saha, S., Moorthi, S., Wu, X., Wang, J., Nadiga, S., Tripp, P., Behringer, D., Hou, Y.-T., Chuang, H.-Y., Iredell, M.,
643   Ek, M., Meng, J., Yang, R., Mendez, M.P., van den Dool, H., Zhang, Q., Wang, W., Chen, M., and Becker, E.: The
644   NCEP climate forecast system version 2. Journal of climate, 27(6), 2185-2208, doi:10.1175/JCLI-D-12-00823.1,
645   2014.

646   Satgé, F., Defrance, D., Sultan, B., Bonnet, M. P., Seyler, F., Rouché, N., and Paturel, J. E.: Evaluation of 23 gridded
647   precipitation datasets across West Africa. Journal of Hydrology, 581, 124412, doi:10.1016/j.jhydrol.2019.124412 ,
648   2020.

649   Sorí, R., Nieto, R., Drumond, A., and Gimeno, L.: The Niger River Basin Moisture Sources: A Lagrangian
650   Analysis. Atmosphere, 8(2), 38, doi: 10.3390/atmos8020038, 2017.

651   Sridevi, C., Singh, K. K., Suneetha, P., Durai, V. R., and Kumar, A.: Rainfall forecast skill of Global Forecasting
652   System (GFS) model over India during summer monsoon 2015. Geofizika, 35(1), 39–52, doi: 10.15233/gfz.2018.35.4,
653   2018.

654   Sylla, M. B., Faye, A., Giorgi, F., Diedhiou, A., and Kunstmann, H.: Projected heat stress under 1.5 C and 2 C global
655   warming scenarios creates unprecedented discomfort for humans in West Africa. Earth's Future, 6(7), 1029-1044, doi:
656   10.1029/2018EF000873, 2018.

657   Tian, D., Wood, E.F., and Yuan, X.: CFSv2-based sub-seasonal precipitation and temperature forecast skill over the
658   contiguous United States. Hydrology and Earth System Sciences, 21, 1477–1490, doi:10.5194/hess-21-1477-2017,
659   2017.

660   Towner, J., Cloke, H.I., Zsoter, E., Flamig, Z., Hoch, J.M., Bazo, J., de Perez, E.C., and Stephens, E.M.: Assessing
661   the performance of global hydrological models for capturing peak river flows in the Amazon basin. Hydrology and
662   Earth System Sciences, 23, 3057–3080, doi:10.5194/hess-23-3057-2019, 2019.

663   van de Giesen, N., Hut, R., & Selker, J.: The trans-African hydro-meteorological observatory (TAHMO). Wiley
664   Interdisciplinary Reviews: Water, 1(4), 341-348, doi:10.1002/wat2.1034, 2014

665   Wang, J. W. A., Sardeshmukh, P. D., Compo, G. P., Whitaker, J. S., Slivinski, L. C., McColl, C. M., and Pegion, P.
666   J.: Sensitivities of the NCEP global forecast system. Monthly Weather Review, 147(4), 1237–1256, doi:
667   10.1175/MWR-D-18-0239.1, 2019.

668   Wang, T., Chu, C., Sun, X., & Li, T.: Improving real-time forecast of intraseasonal variabilities of Indian summer
669   monsoon precipitation in an empirical scheme. Frontiers in Earth Science, 408 doi: 10.3389/feart.2020.577311, 2020.

670   Xu, L., Chen, N., Zhang, X., Chen, Z., Hu, C., & Wang, C.: Improving the North American multi-model ensemble
671   (NMME) precipitation forecasts at local areas using wavelet and machine learning. Climate dynamics, 53(1), 601-
672   615, doi: 10.1007/s00382-018-04605-z, 2019.

673   Yu, P. S., Yang, T. C., Chen, S. Y., Kuo, C. M., & Tseng, H. W.: Comparison of random forests and support vector
674   machine for real-time radar-derived rainfall forecasting. Journal of Hydrology, 552, 92-104, doi:
675   10.1016/j.jhydrol.2017.06.020, 2017.

676   Yuan, X., E. F. Wood, and M. Liang: Integrating weather and climate prediction: toward seamless hydrologic
677   forecasting. Geophysical Research Letters, 41, 5891–5896, doi:10.1002/2014GL061076, 2914.

678   Zhang, C., Xue, M., Supinie, T. A., Kong, F., Snook, N., Thomas, K. W., Brewster, K., Jung, Y., Harris, L.M. and
679   Lin, S. J.: How well does an FV3-based model predict precipitation at a convection-allowing resolution? Results from
680   CAPS forecasts for the 2018 NOAA hazardous weather test bed with different physics combinations. Geophysical
681   Research Letters, 46(6), 3523-3531, doi:10.1029/2018GL081702, 2019.

682